1-1-2021

Semi-Resistive Approach for Tightly Coupled Dipole Array Bandwidth Enhancement

Maxence Carvalho
Florida International University

Alexander D. Johnson
Florida International University

Elias A. Alwan
Florida International University

John L. Volakis
Florida International University

IEEE Open Journal of
Antennas and Propagation

Received 3 November 2020; revised 17 December 2020; accepted 18 December 2020. Date of publication 25 December 2020; date of current version 15 January 2021.

Digital Object Identifier 10.1109/OJAP.2020.3047494

Semi-Resistive Approach for Tightly Coupled Dipole Array Bandwidth Enhancement

MAXENCE CARVALHO (Graduate Student Member, IEEE), ALEXANDER D. JOHNSON (Member, IEEE), ELIAS A. ALWAN (Member, IEEE), AND JOHN L. VOLAKIS (Fellow, IEEE)

Department of Electrical and Computer Engineering, Florida International University, Miami, FL 33174, USA

CORRESPONDING AUTHOR: M. CARVALHO (e-mail: mcarvalh@fiu.edu)

ABSTRACT A new approach to enhance the bandwidth of Tightly Coupled Dipole Arrays (TCDA) is presented. The new design achieves the integration of a semi-resistive Frequency Selective Surface network (FSS) composed of a non-resistive low-pass FSS and two resistive band-stop FSSs. The integration of this FSS network within a dual-polarized Tightly Coupled Dipole Array (TCDA) led to an increased impedance bandwidth of 28:1 from 0.20GHz to 5.6GHz. Notably, the use of an FSS superstrate allowed for scanning down to 60° at VSWR $<$ 3 in the E-plane and VSWR $<$ 4 in the D- and H-planes. Additionally, the strategic use of the inserted low-pass FSS reduces the resistive effects above 2.5GHz for improved average efficiency. A 12×12 array prototype was fabricated and tested to verify the bandwidth and gain of a finite array. The simulated radiation efficiency was demonstrated to be 83%, on average, across the band.

INDEX TERMS Tightly coupled dipole array (TCDA), ultra-wideband (UWB) array, phased array, frequency selective surface (FSS) network, wide-angle impedance matching (WAIM), bandwidth enhancement.

I. INTRODUCTION

THE GROWING interest for small space communication platforms (CubeSats) with increased data throughput and broad spectrum coverage implies a need for low-profile UWB arrays capable of more than 10:1 impedance bandwidth [1]–[3]. To this end, Tightly Coupled Dipole Arrays (TCDA) capable of greater than 10:1 impedance bandwidth have been proposed. In addition to the tightness between nearby dipoles, another critical aspect of the TCDAs is the integration of unbalanced to balanced feed (balun) within a single board [4]–[6]. These baluns are capable of suppressing common-modes across a wide bandwidth while concurrently performing a 4:1 impedance transformation. Other types of wideband arrays are the Frequency-Scaled Ultra-wide Spectrum Elements (FUSE) and employ carefully placed shorting pins and H-Walls [7]. Recently, Wide Angle Impedance Matching (WAIM) layers were introduced with TCDAs for greater bandwidth while scanning [8]–[9]. These artificial substrate loadings exhibit anisotropy and are essentially paired with connected slot arrays to extend their bandwidth up to an octave [10]–[12]. Despite all these improvements, low-profile TCDA still exhibits less bandwidth as compared to tapered slot arrays unless resistive loading is used the aperture efficiency is reduced [13]. Notably, TCDAs have better polarization purity and much lower profile, but recent works are considering reducing cross-polarization on tapered slot arrays [14]–[16]. To further increase TCDA bandwidth, previous designs incorporated uniform resistive FSS. These designs exhibited periodic attenuation at ground plane resonance locations and the added bandwidth was achieved by lowering efficiency across the entire frequency range [17]–[21].

In this communication, we introduce a revised version of a resistively loaded TCDA that exhibits a wider bandwidth with higher average efficiency across the frequency band. Notably, our design integrates a semi-resistive FSS network that concurrently suppresses ground plane shorts and preserves the higher frequency band from losses. The presented array is dual-polarized and operates from 0.20 to 5.6 GHz with a VSWR $<$ 3 down to 60° scanning in the E-plane and 45° in the D- and H- planes. This is achieved using a triple-layer semi-resistive FSS Network between the ground plane and the radiators as seen in Figs. 1 and 2. The design exhibits excellent cross-polarization performance.

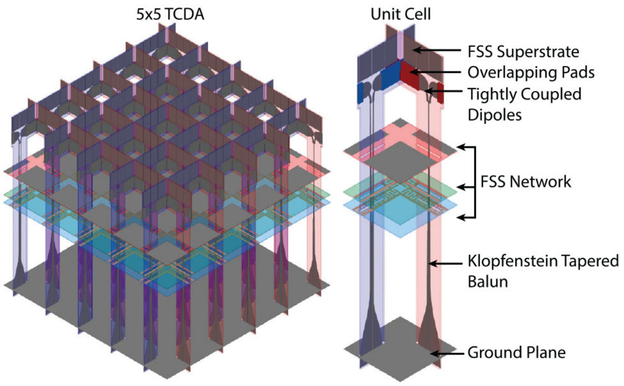

FIGURE 1. Unit cell detail of the novel semi-resistively loaded TCDA. A 5 × 5 array illustrates the egg-crate arrangement of the array.

A 12 × 12 element prototype was fabricated and measured to verify the performance. It is also worth mentioning that the aperture thickness from the top of the WAIM-FSS to the bottom of the connector is only $0.069\lambda_{low}$, where λ_{low} is the wavelength at the lowest operating frequency of 200 MHz.

This communication is organized as follows. Section II introduces the design approach and the proposed FSS network. Section III presents the measurements of a 12 × 12 prototype and Section IV discusses further improvements. In summary, the proposed design provides a proof of concept to extend the bandwidth of TCDAs without appreciably reducing efficiency across the operational frequency range.

II. ARRAY DESIGN AND SIMULATION

A. ARRAY AND FSS SUPERSTRATE DESIGN

As seen in Fig. 2, the dipoles, feed structure, and WAIM-FSS are designed on a single 2-layers Rogers 4003 board of thickness t = 0.305 mm and inserted vertically against the ground plane. The dipole arms reside in the center Rogers layer, and the capacitive overlapping arms are placed at the outer layers to achieve the current sheet effect between adjacent dipoles. The capacitive coupling is controlled by fine-tuning the length (L_c) and width (W_c) of the overlapping metal pads forming the dipole and the capacitive pads. Additionally, the FSS superstrate (WAIM-FSS) is designed for low scanning angles. This superstrate FSS exhibits a cut-off frequency beyond those of the dipole array and serves to emulate an equivalent dielectric constant, ϵ_{Eq}. Hence, it serves to lower the impedance mismatch between the dipoles and free-space [8], [22]. The WAIM-FSS length, h_w, width d_w and, pitch s_w are key parameters (See Fig. 2 and Fig. 4) to fine-tune its equivalent impedance Z_{FSS} looking into the ground plane from the array plane. Importantly, the overall structure is packaged in a thickness smaller than $\lambda_{low}/14.5$, measured from the bottom of the feed connectors to the top of the WAIM-FSS layers. In cohesion with previous designs, the proposed novel semi-resistive FSS network in the substrate simulates an intermediate ground plane for higher frequencies while canceling reflections in the lower band for optimized efficiency. As noted, the proposed novel semi-resistive FSS network represents an electrically variable ground plane thickness to ensure congruent radiation. Notably, this is the first TCDA with a 28:1 broadside bandwidth and an average radiation efficiency greater than 83%. Fabrication details are discussed in Section III.

B. ARRAY AND FSS SUPERSTRATE DESIGN

Essential to the triple-layer FSS substrate are the frequency characteristics of the low-pass FSS at the top in Figs. 1 and 2. Above its cut-off frequency (f_0) this FSS acts as the ground plane itself, leading to ground plane distance control. This enables improved bandwidth and resonance suppression. To further understand the low-pass FSS operation, Fig. 3 depicts its equivalent circuit, assuming a "perfect" band-pass/shielding. At frequencies below cut-off (in green), the radiated wave front propagates through the low-pass FSS and acquires additional transmission phase $\phi_t(f)$ (due to the FSS). Referring to Fig. 3, the wave continues to the ground plane and gets reflected with a reflection phase of π. In its return, it passes again through the FSS and acquires an added phase delay. Further, after propagation of a distance $2h$ a phase of $2kh$ is also added. In total, the overall phase delay of the wave after propagation from the antenna aperture plane to the ground plane and back is

$$\Delta\phi_1 = 2kh + 2\phi_t(f) + \pi \tag{1}$$

In this, h denotes the height of the antenna plane, $\phi_t(f)$ is the transmission phase after going through the low-pass FSS, and k refers to the wavenumber. At frequencies above the low-pass FSS cut-off, the wave is reflected with a phase $\phi_r(f)$. Adding the distance $2d$, the phase delay from the antenna aperture plane to the FSS plane and back is

$$\Delta\phi_2 = 2kd + \phi_r(f) \tag{2}$$

Optimization of the low pass FSS layer (See Fig. 3 for the equivalent circuit) is necessary to guarantee coherent addition of the direct and reflected waves for frequencies above f_1 and f_0. Here, $f_1 = \frac{c_0}{\lambda_1}$ denotes the frequency of the highest observed ground plane resonance. Indeed, if the distance between the FSS and the dipole is $\frac{\lambda_1}{4}$, and considering the frequencies above the FSS cut-off, the first ground plane resonance will occur when $\frac{\lambda_{res}}{2} = \frac{\lambda_1}{4}$. A challenge is to choose the appropriate f_1 so that the resonances in the upper band are removed.

In practice, the frequency response of the FSS exhibits a certain roll-off. From the equivalent transmission line circuit of the lossless low-pass FSS, as in Fig. 3, we can express the transmission phase of the FSS as [23]

$$\phi_t(f) = \tan^{-1}(C_1 \pi Z_0 f) \ = -\tan^{-1}\left(\frac{f}{f_0}\right) \tag{3}$$

Above, C_1 is the equivalent capacitance of the low-pass FSS, and Z_0 denotes the characteristic impedance of free-space (Transmission Line Model). From this, we observe

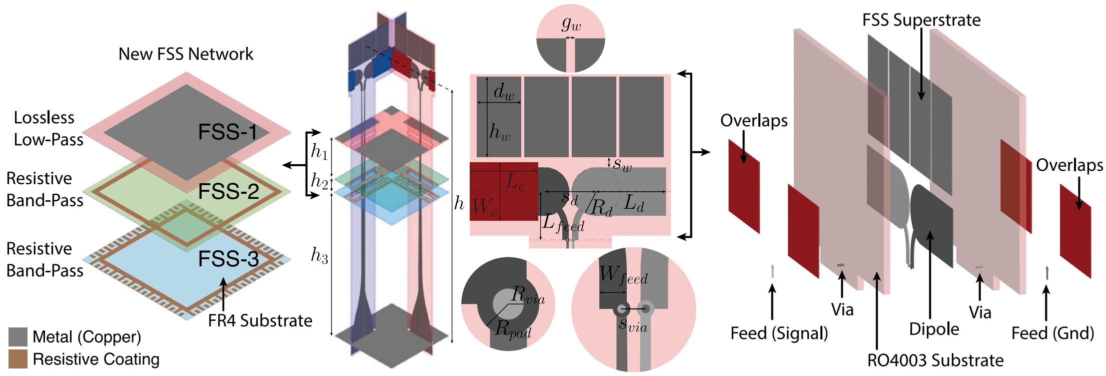

FIGURE 2. Proposed semi-resistively loaded TCDA showing the triple-layer FSS substrate enabling 28:1 impedance bandwidth. Three FSSs are placed at various heights from the ground plane and have suitably designed pass-bands to reconfigure the ground plane electrical thickness. Another innovation of our design is the Klopfenstein tapered balun transitioning to each dipole arm with blind vias for greater bandwidth.

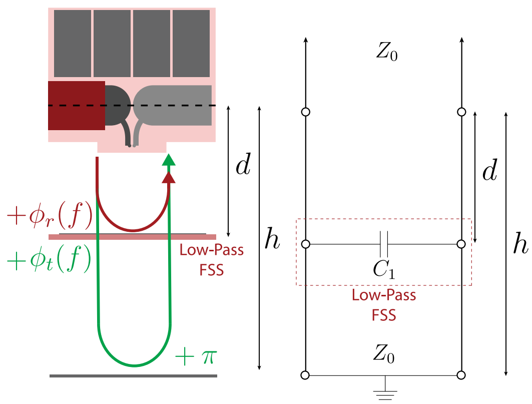

FIGURE 3. Cross section of the TCDA showing the phase paths.

that the transmission phase of the FSS varies between 0 and $\frac{\pi}{4}$ below the cut-off frequency. Therefore, lower frequencies exhibit a delay between 0 and $\frac{\pi}{2}$. This implies that resonances are pushed to the lower band.

C. NOVEL SEMI-RESISTIVE FSS NETWORK

The novel FSS network equivalent circuit is depicted in Fig. 4 and the FSSs Details are shown in Fig. 5. As mentioned earlier, the first FSS (FSS-1) is a lossless low-pass FSS. However, the second (FSS-2) and third (FSS-3) FSSs have resistive loading. The first FSS exhibits a low-pass response with a cut-off frequency (3dB) at 2 GHz. That is, for the lower frequencies, it is more or less transparent. For frequencies above 2 GHz, it becomes reflective and serves as the ground plane's new location. The second FSS is a resistive band-stop ring designed to attenuate the ground plane short at 2 GHz. Notably, it exhibits a peak of attenuation at 2 GHz. The third FSS is a resistive band-stop ring with a peak of attenuation at 0.5 GHz.

Interwoven separations were added around the periphery to minimize its size and remain $< \lambda_{high}/2$. Notably, the increased capacitive coupling between adjacent cells lowers the resonance of the FSS. Both FSS-2 and FSS-3 used resistive loading of $10\Omega/Sq$. As compared to previous resistive FSS designs [18], [19], [24], this novel FSS network limits its losses to restricted bandwidth. That is, it accomplishes a more targeted attenuation, qualifying it as semi-resistive. Overall, the FSS network acts as a low-pass filter for waves propagating towards the ground plane.

The design was optimized using a hybrid full-wave/circuit analysis of the circuit Fig. 4 using both Ansys HFSS and Ansys Circuits. From the TCDA equivalent circuit (left-most graphic) we extracted the dipole and the feed components via full-wave simulations. As seen, a ground-plane free unit cell was isolated and simulated using two Floquet excitations. The top Floquet excitation is located at $\frac{\lambda_{low}}{4}$ away from the dipole plane, where λ_{low} is the lowest frequency of operation. The bottom Floquet excitation is arbitrary located under the usual ground plane location. The phase of the second excitation is de-embedded into the dipole plane to suppress additional phase shifts. That is, the full-wave simulation (center graphic in Fig. 4) characterizes the dipole unit cell comprised of the WAIM-FSS, the overlapping dipoles, and the balun feeds. The optimized dipole was then introduced back into the equivalent circuit. The entire circuit was then used to optimize the FSS network. Each FSS was represented using their respective lumped components equivalent [23], [25]. This approach led to quick optimization and an excellent starting point for full-wave simulations. The final optimized parameters for each FSS unit cell are given in see Fig. 5. They are: $W_1 = 20$ mm, $W_2 = 23$ mm, $W_3 = 23$ mm, $s_2 = 1$ mm, $s_3 = 1$ mm, $g_3 = 0.5$ mm. The overall FSS network performance is plotted in Fig. 6.

D. 30:1 KLOPFENSTEIN TAPERED BALUN

To achieve a greater impedance bandwidth, the array feed must be designed in tandem with the radiating elements. Typically, tapered baluns that are avoided because of their length. However, contrary to the design presented in [5], [26], the proposed balun design combines both mode transduction and impedance transformation similarly to [27]. This approach allows wider bandwidth while limiting the aperture depth under the ground plane ($\lambda_{low}/14.5$), a Klopfenstein tapered profile is designed using a Bézier

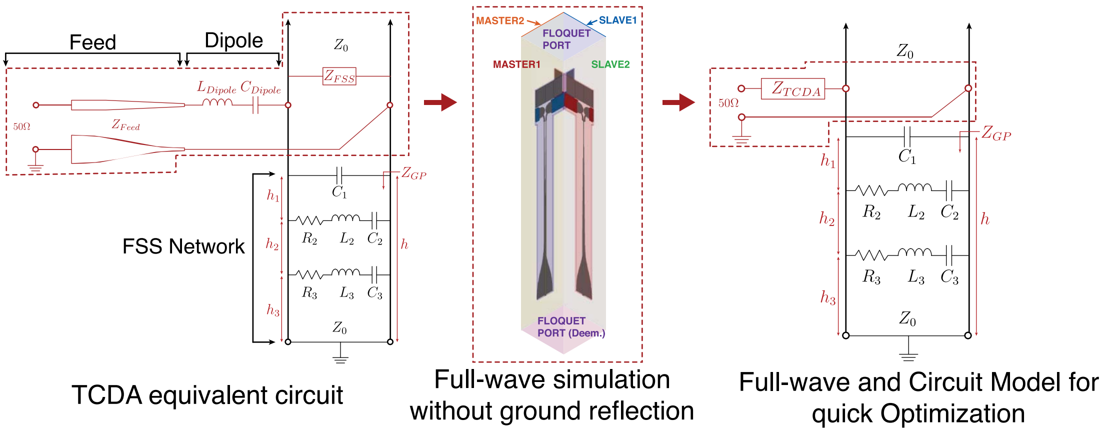

FIGURE 4. Equivalent circuit of the Novel semi-resistively loaded TCDA, showing the FSS-Network equivalent circuit, including the Klopfenstein tapered balun presented later.

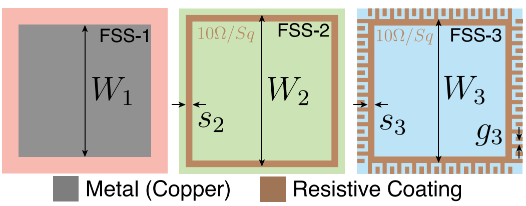

FIGURE 5. Representation of the three FSS unit cell in the TCDA substrate to enable 28:1 impedance bandwidth. From left to right: top Low-pass FSS, resistive ring-shaped stop-band FSS, inter-digitized stop-band FSS. It is noted that, W_1, W_2, and W_3 represent the ring widths of the outer frame of FSS-1, FSS-2 and FSS-3 respectively. The thicknesses of FSS-2 and FSS-3 are controlled by the parameters s_2 and s_3. Further, g_3 represents the pitch between the interwoven teeth of FSS-3. The final dimensions of each layer are $W_1 = 20$ mm, $W_2 = 23$ mm, $W_3 = 23$ mm, $s_2 = 1$ mm, $s_3 = 1$ mm, and $g_3 = 0.5$ mm.

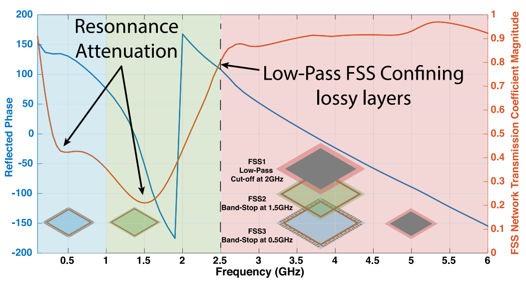

FIGURE 6. Simulated FSS network transmission coefficient and phase response of a plane wave reflected from an infinite ground plane in presence of the FSS semi-resistive network.

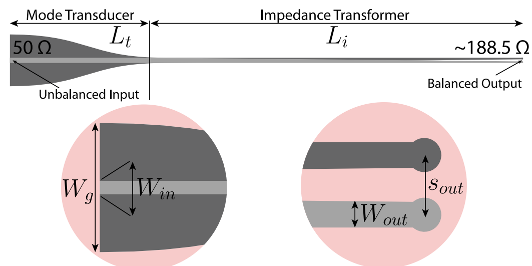

FIGURE 7. Klopfenstein tapered balun comprised of a mode transducer and an impedance transformer. The balun includes a smooth transition from an unbalanced input (50Ω) to a pair of balanced outputs, each exhibiting 188:5Ω.

curve approximation. Such a design involves simplicity (polynomial curve) and efficiency and is better than a classical exponential taper. Also, this design approach is compatible with electromagnetics simulation CAD tools.

The novel balun is depicted in Fig. 7, and is comprised of two parts: A mode transducer and an impedance transformer. By optimizing the transition between the two parts of the balun we can achieve a minimum of reflection. Notably, if the transductive part is too long, the impedance transformation will not be as effective. On the other hand, if it is too short, an abrupt transition from the unbalanced excitation is observed and the differential mode will not be properly excited. Through optimization, more than 15dB insulation between the common and differential modes across the entire band. Concurrently, the input impedance was tapered from 50Ω to $\sim$ 188.5Ω at the dipole terminations. Notably, the extended length of the impedance transformer appears as twin lines, leading to a common-mode resonance between adjacent cells during scanning. However, the low-pass FSS and the resistive loading suppress the common-mode resonance. The final dimensions of the fabricated balun are: $L_t = 30$ mm, $L_i = 69$ mm, $W_g = 10$ mm, $W_{in} = 1$ mm, $W_{out} = 0.3$ mm, $s_{out} = 0.7$ mm.

E. INFINITE ARRAY SIMULATION

An infinite array simulation was realized using the commercially available software ANSYS HFSS. As seen in Fig. 9, the dual-polarized TCDA operates from 0.20 to 5.6 GHz and shows an impressive 28:1 bandwidth with VSWR $<$ 3 at broadside. Also, VSWR $<$ 3 and VSWR $<$ 4 are observed, when scanning down to 60° in the E- and H-plane, respectively. Reduced performance in the H-plane is expected when scanning to low angles due to variations in the dipole array impedance [28]. Such mismatch can be reduced by improving the design of WAIM layers. However, such designs require more complex fabrication and incorporation of horizontal boards. As anticipated, the radiation efficiency matches the attenuation of the FSS network presented in Fig. 6. It shows 2 efficiency lows at 40% and 35% corresponding to the suppression of resonances in the lower

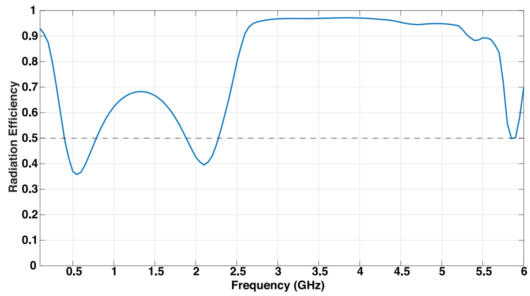

FIGURE 8. Simulated broadside radiation efficiency of the designed TCDA with 28:1 impedance bandwidth.

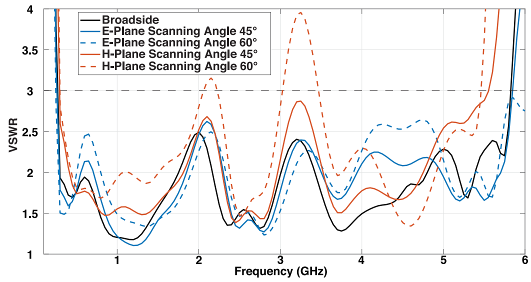

FIGURE 9. Simulated infinite array active VSWR, at broadside radiation and while scanning in both E- and H- planes.

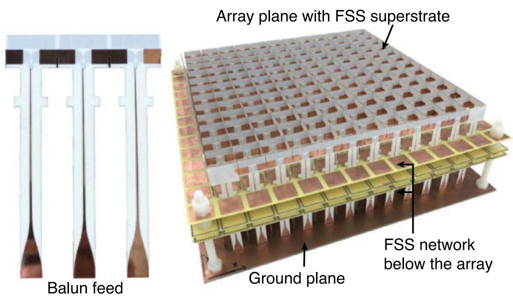

FIGURE 10. Left to right : Fabricated Card with Klopfenstein Tapered Balun, Fabricated 12×12 array with semi-resistive FSS network.

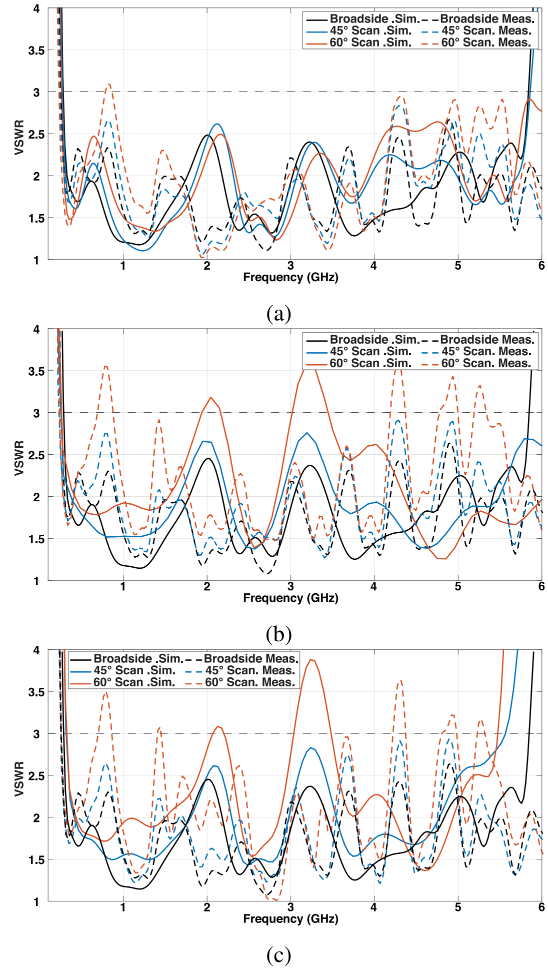

FIGURE 11. Measured and simulated active VSWR of the center TCDA elements at broadside, 45° and 60° scanning. (a) EPlane, (b) D-Plane, (c) H-Plane.

band. Importantly, higher frequencies are barely affected by the resistive loading. This is because the top low-pass FSS "shields" propagation towards the lower resistive FSSs. That is, the novel FSS network suppresses the periodic behavior of the typical R-cards and provides a better-averaged efficiency of 83%. The unit cell dimensions are given in Table 1.

III. PROTOTYPE FABRICATION AND MEASUREMENTS

A. FABRICATED PROTOTYPE

To assess the characteristics of the infinite array, a 12×12 prototype was fabricated. The fabricated array is composed of a 12×1 linear polarized boards, slotted to form the classical egg-crate configuration. The constructed array is depicted in Fig. 10. The boards are comprised of three metal layers of Rogers 4003 material with permittivity $\epsilon_r = 3.55$ and loss tangent $\tan\delta = 0.00027$ and a total thickness of 0.61 mm.

The dipole arms and the scanning FSS are placed in the middle layer and inserted between the overlaps. To assemble the layers, the boards are first adjusted through all the FSS layers as well as the ground plane. Coincident notches are then matching in all the FSS layers as well as the ground plane to insert the TCDA boards. Once the egg-crate is completed, the height of each FSS is adjusted and secured with nylon screws placed at the edge of the array. Notably, the width of the ground and the FSSs are extended to a 14×14 size to allow support by the screws. Additionally, the vertical boards were secured using extra substrate teeth on the side of the balun.

The aforementioned assembly and designs drastically reduce the height between the aperture. As the impedance transformation is mostly done above the ground plane, the remaining aperture depth (under the ground plane) is limited to 5 mm. Also, the mounting process gives more stability and structural resilience. The FSS network is fabricated using 0.51 mm thick FR4. Depending on the application, thicker boards can provide stronger structural rigidity in the middle of the array. If the design was to redo we would recommend using a thicker board to prevent sagging of the boards in the middle of the array.

B. ACTIVE IMPEDANCE MEASUREMENTS

The fabricated array shown in Fig. 10 was used to carry out active impedance measurements using the N5222B Vector

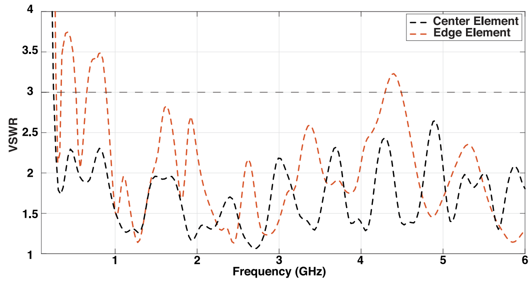

FIGURE 12. Measured broadside VSWR of an off-centered element with comparison to a center element. Ground shorts are observed as the elements get further away from the center.

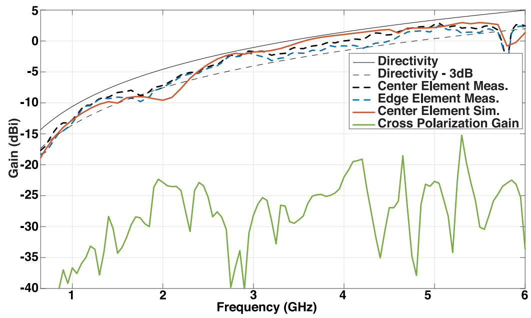

FIGURE 13. Simulated and measured broadside realized gains of a unit cell at different location in the array.

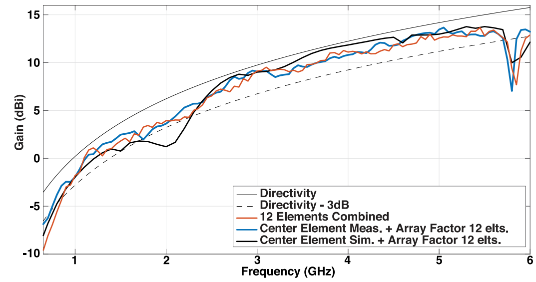

FIGURE 14. Measured broadside co-polarization gain of one central row of the fabricated prototype (12 elements).

TABLE 1. Unit cell dimensions ac cording to Fig. 5 and Fig. 2.

Parameters	Dimensions (mm)	Parameters	Dimensions (mm)
W_1	20	L_d	8.75
W_2	23	R_d	3
W_3	22	s_d	6.3
s_2	1	L_{feed}	6
s_3	1	W_{feed}	0.8
g_3	0.5	R_{via}	0.127
d_w	5.5	s_{via}	0.7
g_w	0.1	R_{pad}	0.254
h_w	10	h	100
s_w	0.125	h_1	15.5
W_c	0.725	h_2	5
L_c	0.85	h_3	55

Network Analyser (VNA). During the measurements, the mutual coupling with neighboring elements was quantified and combined with the return loss of the antenna elements under test. Assuming a uniform feeding and a square lattice, the active S-parameters of the (*p, q*) element is found using the expression in [28]

$$\Gamma_{p,q}(\theta,\ \phi) = \sum_{m=1}^{M}\sum_{n=1}^{N} S_{mn,pq} e^{-jD([m-p]u+[n-q]v)} \tag{4}$$

where $(\theta,\ \phi)$ is the array scan direction, $u = k\sin\theta\cos\phi$ and $v = k\sin\theta\sin\phi$ are the u–v coordinates, and k is the free-space wavenumber. As usual, $S_{mn,pq}$ refer to the measured S-parameters *mn* and pq elements, and M, N and D, are the number of elements along the x and y directions and the lattice spacing.

The measured active central elements VSWR is shown in Fig. 11 alongside infinite array simulations. As seen, measured results match the infinite array simulations and verify the simulated 28:1 impedance bandwidth with VSWR < 3 from 0.20 to 5.6 GHz at broadside. We also observe that scanning down to $\theta = 45°$ is achieved across the 28:1 band in E-plane and down to $\theta = 60°$ in D/H-planes. Good scanning agreement is also seen with some discrepancies for D/H-planes down to $\theta = 60°$, where VSWR spikes of 3.5 and 4 are observed at some frequencies. These discrepancies are attributed to the finite size of the array.

To account for the finite effects, active VSWR measurements of various off-centered elements were also conducted. As depicted in Fig. 12, higher VSWR was observed for off-centered elements. This degraded VSWR is mainly due to edge effects and to lack of surrounding elements. Additionally, the finite aspect of the FSS network is observed as the ground plane short rises. Notably, the further the elements from the center, the FSS network performance is also degrading.

C. FAR-FIELD MEASUREMENTS

Gain measurements were conducted in our near-field anechoic chamber across the 0.650–6 GHz operating band. The measured broadside gain versus frequency for the center and off-centered elements are also included in Fig. 13. The theoretical aperture gain $4\pi A/\lambda^2$ is used as a reference for these measurements. We observe that the center elements gain closely tracks the simulated realized gain. As predicted and as seen in Fig. 13, a maximum drop of 3.1 dB in the measured gain is observed at f = 1.8 GHz. This drop is associated with the reverberation within the substrates as discussed previously. As the simulated efficiency indicates a second and less important radiation efficiency drop is expected around 0.5GHz.

Notably, the measured gain curves show a more efficient operation, giving good agreement with the predicted (and measured) 28:1 VSWR bandwidth. Indeed, the measured array exhibits an improved total efficiency (72% on average). It is also important to note that off-centered elements have a gain similar to the center one with some discrepancy below f = 1 GHz due to higher reflection observed previously in Fig. 12.

To account for the finite effects of the TCDA, the measured broadside gain of a 12×1 elements linear array was also measured and given in Fig. 14. These measurements were conducted using a 12-ways power divider with subsequent post-processing that includes the array factor and

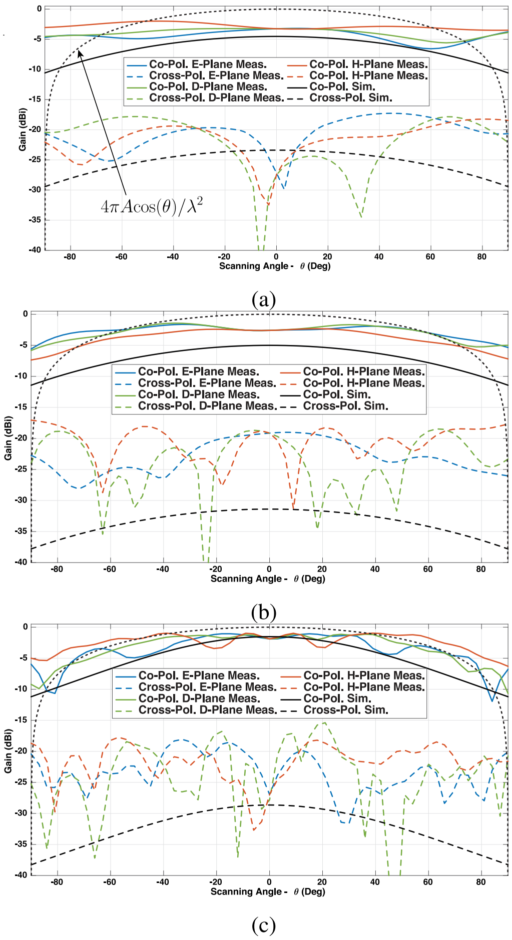

FIGURE 15. Measured embedded patterns of the center array element in E, D, and H planes with comparison to infinite array simulation. (a) 650MHz (b) 2000MHz (c) 5600MHz.

the power divider losses. Notably, the gain measurements for this single board linear array of the TCDA account for finite effects as well as all couplings among the elements. Importantly, the single board gain behavior is similar to the TCDA unit cell gain. That is, it again shows a gain drop at f = 2 GHz

The gain patterns at f = 0.650 GHz, f = 2 GHz and f = 5.6 GHz are presented in Fig. 15(a)–(c) for E-/H-/D-plane, respectively. The theoretical ideal element pattern is also included for reference. Notably, the measured co-polarization patterns closely follow both simulations and theoretical aperture gain of $4\pi\cos\theta A/\lambda^2$. As expected, at f = 650 MHz the beamwidth is wider since the array element is only $\lambda/18$ in aperture size at 650 MHz. Nevertheless, finite array measurements are in good agreement with some discrepancies in the cross-polarization levels. The latter are mostly attributed to the difficulty in achieving perfect alignment during fabrication and measurements. Measurements and simulations show that cross-polarization levels remain more than 15 dB below the co-polarization level. Typically, the observed pattern ripples are due to the finite size of the array. Also, the small pattern asymmetries are due to small asymmetries in the fabricated elements.

TABLE 2. Bandwidth/efficiency trade-off comparison with previous work.

Work	Achieved Bandwidth	Average Efficiency
[18]	21:1	77% (Rad.)
[19]	13.1:1	60% (Total)
[24]	46:1	72% (Rad.)
This work	28:1	83% (Rad.) 72% (Total)

IV. CONCLUSION AND REMARKS

This article presented the design, fabrication, and measurement of a bandwidth enhanced TCDA. This was done by introducing: 1) a triple layer FSS network in the substrate and 2) a new Klopfenstein tapered feed incorporating mode transducer and impedance transformer. The fabricated dual-polarized 12 × 12 array prototype achieved a measured 28:1 contiguous impedance bandwidth (0.20–5.6 GHz) when scanning down to 60° with VSWR < 3 in the E-plane and VSWR < 4 in D- and H-planes. Measurements validated the improved radiation efficiency as compared to past designs. Table 2 shows a comparison of the average efficiencies (Radiation or Total) with previous work. As seen, this work shows for the first time an average total efficiency greater than 70%.

REFERENCES

[1] J. L. Volakis, *Antenna Engineering Handbook*, 5th ed. Columbus, OH, USA: McGraw-Hill Educ., 2018.

[2] R. C. Hansen, *Phased Array Antennas*, 2nd ed. Hoboken, NJ, USA: Wiley, 2009.

[3] E. Kulu. (2020). *Nanosats Database*. [Online]. Available: http://nanosats.eu

[4] J. P. Doane, K. Sertel, and J. L. Volakis, "A wideband, wide scanning tightly coupled dipole array with integrated balun (TCDA-IB)," *IEEE Trans. Antennas Propag.*, vol. 61, no. 9, pp. 4538–4548, Sep. 2013.

[5] A. O. Bah, P.-Y. Qin, R. W. Ziolkowski, Y. J. Guo, and T. S. Bird, "A wideband low-profile tightly coupled antenna array with a very high figure of merit," *IEEE Trans. Antennas Propag.*, vol. 67, no. 4, pp. 2332–2343, Apr. 2019.

[6] J. Zhong, A. Johnson, E. A. Alwan, and J. L. Volakis, "Dual-linear polarized phased array with 9:1 bandwidth and 60° scanning off broadside," *IEEE Trans. Antennas Propag.*, vol. 67, no. 3, pp. 1996–2001, Mar. 2019.

[7] M. W. Elsallal, J. R. Hood, and R. Kindt, "Development of substrate-free frequency-scaled ultra-wide spectrum element (FUSE) phased array," in *Proc. IEEE Int. Symp. Phased Array Syst. Technol. (PAST)*, Waltham, MA, USA, 2016, pp. 1–5.

[8] E. Yetisir, N. Ghalichechian, and J. L. Volakis, "Ultrawideband array with 70° scanning using FSS superstrate," *IEEE Trans. Antennas Propag.*, vol. 64, no. 10, pp. 4256–4265, Oct. 2016.

[9] A. O. Bah, P.-Y. Qin, R. W. Ziolkowski, Q. Cheng, and Y. J. Guo, "Realization of an ultra-thin metasurface to facilitate wide bandwidth, wide angle beam scanning," *Sci. Rep.*, vol. 8, p. 4761, Mar. 2018.

[10] R. M. van Schelven, D. Cavallo, and A. Neto, "Equivalent circuit models of finite slot antennas," *IEEE Trans. Antennas Propag.*, vol. 67, no. 7, pp. 4367–4376, Jul. 2019.

[11] D. Cavallo, W. H. Syed, and A. Neto, "Connected-slot array with artificial dielectrics: A 6 to 15 GHz dual-pol wide-scan prototype," *IEEE Trans. Antennas Propag.*, vol. 66, no. 6, pp. 3201–3206, Jun. 2018.

[12] A. Van Katwijk and D. Cavallo, "Analysis and design of connected slot arrays with artificial dielectrics," in *Proc. IEEE Int. Symp. Phased Array Syst. Technol. (PAST)*, Waltham, MA, USA, 2019, pp. 1–5.

[13] J. P. Doane, K. Sertel, and J. L. Volakis, "Bandwidth limits for lossless, reciprocal PEC-backed arrays of arbitrary polarization," *IEEE Trans. Antennas Propag.*, vol. 62, no. 5, pp. 2531–2542, May 2014.

[14] J. T. Logan, R. W. Kindt, and M. N. Vouvakis, "A 1.2–12 GHz sliced notch antenna array," *IEEE Trans. Antennas Propag.*, vol. 66, no. 4, pp. 1818–1826, Apr. 2018.

[15] J. T. Logan, R. W. Kindt, and M. N. Vouvakis, "Low cross-polarization vivaldi arrays," *IEEE Trans. Antennas Propag.*, vol. 66, no. 4, pp. 1827–1837, Apr. 2018.

[16] R. W. Kindt and J. T. Logan, "Dual-polarized metal-flare sliced notch antenna array," *IEEE Trans. Antennas Propag.*, vol. 68, no. 4, pp. 2666–2674, Apr. 2020.

[17] Y. E. Erdemli, K. Sertel, R. A. Gilbert, D. E. Wright, and J. L. Volakis, "Frequency-selective surfaces to enhance performance of broad-band reconfigurable arrays," *IEEE Trans. Antennas Propag.*, vol. 50, no. 12, pp. 1716–1724, Dec. 2002.
[18] W. F. Moulder, K. Sertel, and J. L. Volakis, "Superstrate-enhanced ultrawideband tightly coupled array with resistive FSS," *IEEE Trans. Antennas Propag.*, vol. 60, no. 9, pp. 4166–4172, Sep. 2012.
[19] D. K. Papantonis and J. L. Volakis, "Dual-polarized tightly coupled array with substrate loading," *IEEE Antennas Wireless Propag. Lett.*, vol. 15, pp. 325–328, 2015.
[20] N. J. Smith, D. Papantonis, and J. L. Volakis, "Bandwidth reconfigurable metamaterial arrays," *Int. J. Antennas Propag.*, vol. 2014, Jun. 2014, Art. no. 397576.
[21] Z. Szabó, G.-H. Park, R. Hedge, and E.-P. Li, "A unique extraction of metamaterial parameters based on Kramers–Kronig relationship," *IEEE Trans. Microw. Theory Techn.*, vol. 58, no. 10, pp. 2646–2653, Oct. 2010.
[22] S. M. A. M. H. Abadi and N. Behdad, "Design of wideband, FSS-based MultiBeam antennas using the effective medium approach," *IEEE Trans. Antennas Propag.*, vol. 62, no. 11, pp. 5557–5564, Nov. 2014.
[23] A. D. Johnson, J. Zhong, S. B. Venkatakrishnan, E. A. Alwan, and J. L. Volakis, "Phased array with low-angle scanning and 46:1 Bandwidth," *IEEE Trans. Antennas Propag.*, vol. 68, no. 12, pp. 7833–7841, Dec. 2020.
[24] Y. Xu and M. He, "Design of multilayer frequency-selective surfaces by equivalent circuit method and basic building blocks," *Int. J. Antennas Propag.*, vol. 2019, Aug. 2019, Art. no. 9582564.
[25] A. O. Bah, P.-Y. Qin, and Y. J. Guo, "An extremely wideband tapered balun for application in tightly coupled arrays," in *Proc. IEEE-APS Topical Conf. Antennas Propag. Wireless Commun. (APWC)*, Cairns, QLD, Australia, 2016, pp. 162–165.
[26] G. Engargiola. (2001). *Tapered Microstrip Balun for ATA Feed Development. ATA Memo 35 Rev 1*. [Online]. Available: http://astro.berkeley.edu/ral/ata/memos/memo35r1.pdf
[27] H. Wheeler, "Simple relations derived fom a phased-array antenna made of an infinite current sheet," *IEEE Trans. Antennas Propag.*, vol. 13, no. 4, pp. 506–514, Jul. 1965.
[28] N. Amitay, V. Galindo, and C. P. Wu, *Theory and Analysis of Phased Array Antennas*. Nashville, TN, USA: Wiley, 1972.

MAXENCE CARVALHO (Graduate Student Member, IEEE) was born in Clermont-Ferrand, France, in 1994. He received the M.Sc. degree in aeronautical and spatial telecommunications from l'École National de l'Aviation Civile, Toulouse, France, in 2018. He is currently pursuing the Ph.D. degree with the RFCOM Laboratory, Florida International University, Miami, FL, USA. His current research interests include ultra-wideband arrays, millimeter-wave technologies for imaging applications, and reconfigurable antennas.

ALEXANDER D. JOHNSON (Member, IEEE) received the B.S. degree in electrical engineering from Western New England University, Springfield, MA, USA, in 2016, the M.S. degree in electrical engineering from the Ohio State University, Columbus, OH, USA, in 2017, and the Ph.D. degree in electrical and computer engineering from Florida International University (FIU), Miami, FL, USA, in 2019. He has been a part-time Principal Scientist with BAE Systems, Nashua, NH, USA, and a Research Assistant Professor with FIU, since August 2019. His research interests include novel materials, textile electronics, wideband array apertures, mm-wave phased arrays, and simultaneous transmit and receive systems. He was recipient of the NASA Research Announcement Fellowship Award in 2018. He also received an Honorable Mention in the Student Paper Competition at the 2019 IEEE Antenna and Propagation Symposium (AP-S/URSI), and the Student Fellowship Travel Grant Award at the U.S. National Committee for the International Union of Radio Science (USNC–URSI) in 2017 and 2018.

ELIAS A. ALWAN (Member, IEEE) was born in Aitou, Lebanon, in 1984. He received the B.E. degree (*summa cum laude*) in computer and communication engineering from Notre Dame University–Louaize, Zouk Mosbeh, Lebanon, in 2007, the M.E. degree in electrical engineering from the American University of Beirut, Beirut, Lebanon, in 2009, and the Ph.D. degree in electrical and computer engineering from the Ohio State University, Columbus, OH, USA, in 2014, where he was a Senior Research Associate with the ElectroScience Laboratory, from 2015 to 2017. He is currently an Assistant Professor with the ECE Department, Florida International University. His research interests include the areas of antennas and radio frequency systems with a particular focus on ultra-wideband (UWB) communication systems, including UWB arrays, reduced hardware, and power-efficient communication back-ends, and millimeter-wave technologies for 5G applications. Since 2010, he has been a Phi Kappa Phi Member.

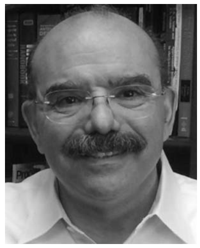

JOHN L. VOLAKIS (Fellow, IEEE) was born in Chios, Greece, in May 13, 1956. He received the B.E. degree (*summa cum laude*) from Youngstown State University, Youngstown, OH, USA, in 1978, and the M.Sc. and Ph.D. degrees from Ohio State University, Columbus, OH, USA, in 1979 and 1982, respectively. He started his career with Rockwell International (1982–1984), now Boeing Phantom Works. In 1984, he was appointed as an Assistant Professor with the University of Ann Arbor, MI, USA, becoming a Full Professor in 1994. He also served as the Director of the Radiation Laboratory from 1998 to 2000. From January 2003 to July 2017, he served as the Roy and Lois Chope Chair Professor of engineering with Ohio State University, and also as the Director of the ElectroScience Laboratory. Since July 2017, he has been serving as the Dean of Engineering with Florida International University. He has authored or coauthored more than 280 articles in major refereed journals, nearly 500 conference papers, and 20 book chapters. He has coauthored the following six books: *Approximate Boundary Conditions in Electromagnetics* (Institution of Electrical Engineers, London, 1995), *Finite Element Method for Electromagnetics* (IEEE Press, 1998), *Frequency Domain Hybrid Finite Element Methods in Electromagnetics* (Morgan & Claypool, 2006), *Computational Methods for High-Frequency Electromagnetic Interference* (Verlag, 2009), *Small Antennas* (McGraw-Hill, 2010), and edited the *Antenna Engineering Handbook* (McGraw-Hill, 2007). He has also written several well-edited coursepacks on introductory and advanced numerical methods for electromagnetics and has delivered short courses on antennas, numerical methods, and frequency selective surfaces. His primary research deals with antennas, computational methods, electromagnetic compatibility and interference, propagation, design optimization, RF materials, multiphysics engineering, and bioelectromagnetics. He was a recipient of the University of Michigan (UM) College of Engineering Research Excellence Award in 1998, the UM Department of Electrical Engineering and Computer Science Service Excellence Award in 2001, and the Ohio State University Clara and Peter Scott Award for Outstanding Academic Achievement in 2010. He is listed by ISI as among the top 250 most referenced authors. He graduated/mentored nearly 85 Ph.D. students/postdocs, and coauthored with them 14 best paper awards at conferences. He was the 2004 President of the IEEE Antennas and Propagation Society and served on the AdCom of the IEEE Antennas and Propagation Society from 1995 to 1998. He chaired the 1993 IEEE Antennas and Propagation Society Symposium and Radio Science Meeting and co-chaired the same symposium in 2003 in Columbus. He also served as an Associate Editor for the IEEE TRANSACTIONS ON ANTENNAS AND PROPAGATION from 1988 to 1992, *Radio Science* from 1994 to 1997, the *IEEE Antennas and Propagation Society Magazine* from 1992 to 2006, the *Journal of Electromagnetic Waves and Applications*, and *URSI Bulletin*. He was elected as a Fellow of the IEEE in 1996 and is a member of the URSI Commissions B and E.